

DOI: 10.1093/genetics/iyab116 Advance Access Publication Date: 9 August 2021 Investigation Highlighted Article

Mitochondrial mutations in *Caenorhabditis elegans* show signatures of oxidative damage and an AT-bias

Gus Waneka, 1,* Joshua M. Svendsen, 1 Justin C. Havird (D), 2 and Daniel B. Sloan (D) 1

Abstract

Rapid mutation rates are typical of mitochondrial genomes (mtDNAs) in animals, but it is not clear why. The difficulty of obtaining measurements of mtDNA mutation that are not biased by natural selection has stymied efforts to distinguish between competing hypotheses about the causes of high mtDNA mutation rates. Several studies which have measured mtDNA mutations in nematodes have yielded small datasets with conflicting conclusions about the relative abundance of different substitution classes (i.e., the mutation spectrum). We therefore leveraged Duplex Sequencing, a high-fidelity DNA sequencing technique, to characterize de novo mtDNA mutations in C meant C magnitude more mtDNA mutations than documented in any previous nematode mutation study. Despite an existing extreme AT bias in the C elegans mtDNA (75.6% AT), we found that a significant majority of mutations increase genomic AT content. Compared to some prior studies in nematodes and other animals, the mutation spectrum reported here contains an abundance of $CG \rightarrow AT$ transversions, supporting the hypothesis that oxidative damage may be a driver of mtDNA mutations in nematodes. Furthermore, we found an excess of $C \rightarrow T$ and $C \rightarrow T$ changes on the coding DNA strand relative to the template strand, consistent with increased exposure to oxidative damage. Analysis of the distribution of mutations across the mtDNA revealed significant variation among protein-coding genes and as well as among neighboring nucleotides. This high-resolution view of mitochondrial mutations in C elegans highlights the value of this system for understanding relationships among oxidative damage, replication error, and mtDNA mutation.

Keywords: mutation spectra; replication error; oxidative damage; cytosine deamination; oxidized guanine; mitochondrial mutation; metazoan mtDNA; low-frequency variant; Duplex Sequencing; mutation accumulation

Introduction

Mitochondrial genomes (mtDNAs) of most animals have mutation rates about one order of magnitude greater than their corresponding nuclear genomes (Wolfe et al. 1987; Denver et al. 2000, 2004; Havird and Sloan 2016; Allio et al. 2017). While rapid mtDNA mutation rates of metazoans have proven useful for understanding the divergence of closely related species (Bernt et al. 2013; Yang et al. 2016), they also pose a serious challenge for organismal fitness (Gemmell et al. 2004). In humans, mtDNA mutations cause genetic disorders (Longley et al. 2005; Marni and Soondhiemer 2010), are associated with numerous cancers (Gorelick et al. 2021) and accumulate with age (Kennedy et al. 2013). Furthermore, individuals suffering from age-related diseases such as Parkinson's and Alzheimer's display increased mtDNA mutations compared to healthy individuals (Monzio Compagnoni et al. 2020). The mechanisms underlying high mtDNA mutation rates in metazoans remain the subject of ongoing research and debate.

Historically, elevated mtDNA mutation rates have been hypothesized to be driven by oxidative damage (Harman 1972; Miquel et al. 1980; Richter et al. 1988; Shigenaga et al. 1994) from

reactive oxygen species (ROS), which are abundant byproducts of electron transport in the mitochondria (Murphy 2009). Several studies measuring mtDNA mutations in metazoans have raised doubts about the oxidative damage hypothesis. Specifically, genetic backgrounds with increased ROS do not show a detectable increase in mtDNA mutations (Itsara et al. 2014), nor do those with deficiencies in oxidative damage repair machinery (Halsne et al. 2012; Itsara et al. 2014; Kauppila et al. 2018). In addition, the mtDNA mutation spectra from humans is relatively deplete of CG→AT transversions (Kennedy et al. 2013), a substitution class considered a hallmark of oxidative damage (Cheng et al. 1992; Kirkwood and Kowald 2012).

Alternatively, high metazoan mtDNA mutation rates may be driven by replication errors or deficiencies in mtDNA repair machinery (Longley et al. 2005; Szczepanowska and Trifunovic 2015; DeBalsi et al. 2017; Hood et al. 2019). The replication error hypothesis is supported by in vitro mtDNA replication assays with Pol γ (the metazoan mtDNA polymerase), which recapitulate most (83%) of the mutational hotspots detected in a portion of the human mitochondrial genome through phylogenetic methods (Zheng et al. 2006). The in vivo mtDNA mutational spectra of

¹Department of Biology, Colorado State University, Fort Collins, CO 80523, USA and

²Department of Integrative Biology, University of Texas at Austin, Austin, TX 78712, USA

^{*}Corresponding author: Biology Department, Colorado State University, Fort Collins, CO, USA. Email: gus.waneka@gmail.com

humans, fruit flies, and mice, are all dominated by CG→TA transitions, which are commonly attributed to Pol γ error (Zheng et al. 2006; Kennedy et al. 2013; Itsara et al. 2014; Melvin and Ballard 2017; Arbeithuber et al. 2020). However, because cytosine deamination (to uracil) is likely a major cause of CG→TA transitions in metazoan mtDNAs, the high abundance of these substitutions may reflect a complex relationship between single-stranded DNA damage, failed DNA repair, and replication error. Deamination of cytosine can occur via spontaneous hydrolysis (Nabel et al. 2012), but oxidative damage can also play a role by creating modified bases that are more prone to deamination and/or less accessible to repair pathways (Kreutzer and Essigmann 1998). It is not clear whether cytosine deamination in metazoan mtDNAs is driven by spontaneous hydrolysis, oxidative damage, or a combination of the two. If deaminated cytosines are not repaired through base excision repair (BER), Pol γ frequently incorporates adenine opposite of uracil during DNA replication (Zheng et al. 2006). In a successive round of DNA replication, the pairing of thymine with adenine completes the double-stranded $CG \rightarrow TA$ transition (Nabel et al. 2012). The role of deamination in CG→TA transitions in metazoan mtDNAs is supported by strand asymmetry analyses, which have revealed significantly higher frequencies of C→T than G→A changes on mtDNA strands that spend increased time in single-stranded states during mtDNA replication (Kennedy et al. 2013; Itsara et al. 2014; Ju et al. 2014; Arbeithuber et al. 2020; Sanchez-Contreras et al. 2021). Such asymmetric single-stranded exposure likely explains why the C-T change occurs on the "minor strand" in 91% of CG→TA transitions in fruit fly mtDNA (Itsara et al. 2014). Interactions between damage and polymerase fidelity can be difficult to untangle. For example, a recent study showed the in vitro proofreading activity of human Pol y decreased when oxidative stress was applied to the enzyme (Anderson et al. 2020).

A major obstacle in understanding causes of metazoan mtDNA mutations stems from the difficulty of detecting rare mutation events and removing the biasing effects of selection. Mutation accumulation (MA) experiments (Katju and Bergthorsson 2019) have been used to address this challenge in fruit flies (Haag-Liautard et al. 2008; Keightley et al. 2009), mice (Uchimura et al. 2015), water fleas (Xu et al. 2012) and most extensively, nematodes (Denver et al. 2000; Howe et al. 2010; Molnar et al. 2011; Konrad et al. 2017; Wagner et al. 2020). MA studies remove the filtering effects of natural selection by bottlenecking experimental lines through randomly selected individuals for successive generations. Under these conditions, nonlethal mutations are expected to accumulate and can be assayed through genome resequencing of the final MA generation. However, while MA experiments have proven extremely useful for studying mutation (Lynch et al. 2016), this approach poses special challenges for measuring mtDNA mutations (Schaack et al. 2020). Mitochondrial genomes remain multicopy throughout the entirety of metazoan germline development (Bratic et al. 2010; Wai et al. 2010), giving selection the opportunity to act on competing mtDNAs within an individual (Fan et al. 2008), even during MA experiments (Schaack et al. 2020). The polyploid nature of mtDNAs means that new mutations are born into a low frequency, heteroplasmic state (multiple haplotypes within the same mitochondria or individual). New mtDNA mutations must therefore rise in frequency (through drift or selection; Schaack et al. 2020) in order to meet the detection thresholds set by the high error rates (often above 10⁻³ errors per bp) of traditional DNA sequencing methods (Schirmer et al. 2016).

Two large-scale MA experiments with the nematode Caenorhabditis elegans have reached very different conclusions

regarding the spectrum of mtDNA mutations (Denver et al. 2000; Konrad et al. 2017). The pioneering study of Denver et al. (2000) was the first MA experiment to characterize mtDNA mutations in metazoans, using Sanger sequencing to detect a total of 26 mutations in 74 MA lines bottlenecked for an average of 214 generations. The 16 single nucleotide variants (SNVs) they identified indicated a bias towards mutations that increase GC content (10 variants increased GC content, four decreased GC content and two were GC neutral), a surprising finding given that the C. elegans mtDNA is 75.6% AT. However, a more recent C. elegans MA experiment utilized Illumina sequencing to detect a total of 24 mtDNA mutations (nine SNVs) in 20 MA lines each bottlenecked for an average of 363 generations and found a strong bias in the opposite direction; eight of nine SNVs increased AT content, and the other SNV was AT neutral (Konrad et al. 2017). Both of these studies were impressive, multi-year undertakings, and it is unclear whether the differences in the reported spectra are driven by biological differences in the C. elegans lines or rearing conditions, differences in sequencing techniques, or noise associated with small sample sizes. Additional MA experiments conducted with the nematodes Caenorhabditis briggsae (Howe et al. 2010; Wagner et al. 2020) and Pristionchus pacifics (Molnar et al. 2011) have also yielded very few mutations (7-19 SNVs), making it difficult to get precise estimates of mutation parameters.

An alternative to MA experiments has emerged in the form of high-fidelity sequencing techniques that can detect mtDNA variants segregating in tissues at extremely low frequencies (Salk et al. 2018; Sloan et al. 2018). One technique called Duplex Sequencing (Schmitt et al. 2012; Kennedy et al. 2014) is particularly useful for this application as it is highly accurate with error rates as low as $\sim 2 \times 10^{-8}$ per bp (Wu et al. 2020), facilitating detection of de novo mtDNA mutations essentially as they occur. Duplex Sequencing works by tagging both ends of library molecules with random barcodes before they are amplified and sequenced. These barcodes are then used to create families of reads corresponding to each of the original strands from a parent DNA fragment. Consensus base calling eliminates variants present only in a minority of reads within a family or only in reads originating from one of the two strands, as such variants are common artifacts of single-stranded DNA damage, PCR misincorporations, and sequencing error. Here, we employed hybridization-based mtDNA enrichment coupled with Duplex Sequencing to greatly increase the detection of de novo mutations and better characterize the spectrum and distribution of mutations in the C. elegans mitochondrial genome.

Materials and methods

Nematode growth and DNA extraction

Replicate cultures of nematodes were derived from the Bristol N2 strain of C. elegans and grown on nematode growth media (NGM; He 2011) plates with Escherichia coli strain OP50 at 20°C. Our nematode rearing protocol (outlined in Supplementary Figure S1) was designed to (1) sample a diverse tissue pool comprised of many individuals (i.e., with a diversity of rare mtDNA mutations), (2) target lineages separated from each other for multiple generations to limit the contribution of shared, heteroplasmic mtDNA variants, and (3) limit the total number of generations (to three) in order to minimize potential biases of selection. Three siblings (F0) worms were randomly chosen from our stock of N2 nematodes to initiate experimental populations (referred to hereafter as populations 1, 2, and 3). Each population was maintained for 15 generations, with passages of ten adults at each generation, before a single adult F15 founder was randomly selected and transferred to a fresh NGM plate. Three F16 progeny were then randomly chosen from each population to initiate the nine replicates assayed in this study (referred to hereafter as replicates 1a, 1b, 1c, 2a, 2b, 2c, 3a, 3b, and 3c). Each replicate culture was allowed to proliferate for three generations (14-16 days) before all offspring in a replicate (mixed-stage individuals) were pooled for DNA extraction.

The three replicates from each population were grown in parallel, and the different populations were grown in three sequential batches. All culturing conditions and plate transfers followed the same outline (Supplementary Figure S1). The replicates were checked daily to monitor growth and food supply. After each generation, worms were collected in M9 liquid buffer (He 2011), pelleted by centrifugation at 1900 rcf for 30 seconds, and redistributed onto fresh NGM plates. The first replating took place 7–9 days after the F16 replicate founder was plated. The F17 progeny were collected and redistributed onto 3 new plates. During this replating, one-third of the worms were discarded so as not to overwhelm the food supply on the new plates. To ensure this culling step did not result in a biased sampling of the population, we homogenized each worm pellet with gentle pipetting before discarding a third of the pellet by volume. Three to six days later, the F18 worms were collected from the 3 plates (per each replicate) and pooled before half of the worms were discarded (again, so as not to overwhelm the food supply on the new plates), and the other half were redistributed onto 10 new NGM plates (per each replicate) for the final stage of growth. After 2-3 days, the F19 worms were collected from all 10 plates (per each replicate) and pooled into one 15 ml falcon tube (per each replicate). The worms were pelleted by centrifugation at 1900 rcf for 30 seconds, and the supernatant was discarded. Then, M9 buffer was used to resuspend the worms, and the wash process was repeated 2 more times to deplete contaminating E. coli. Totalcellular DNA was extracted from the worm pellet using the DNeasy Blood and Tissue Kit (Qiagen), following manufacturer's instructions.

Duplex library preparation and mtDNA enrichment

Total cellular DNA was stored at −20°C until all 9 replicates were processed. Then, Duplex Sequencing libraries were created for all 9 samples, following our previously described protocols (Wu et al. 2020) with some modifications. Briefly, DNA was fragmented with a Covaris M220 Focused-Ultrasonicator, end repaired (NEBNext End Repair Module), and A-tailed (Klenow Fragment Enzyme, 1 mM dATP). The A-tailed DNA was then adaptor ligated with custom Duplex adaptors, which contain the 12-bp random barcodes necessary for double-stranded consensus building. The adaptor-ligated product was treated with a cocktail of three repair enzymes (Uracil-DNA Glycosylase, Fpg, and Endonuclease III in NEB CutSmart Buffer) to remove fragments with singlestranded damage and 16 ng of repaired DNA was used as input for the first round of PCR (13 cycles), in which Illumina adaptors with multiplexing indices were incorporated into the amplicons (NEBNext Ultra II Q5 Master Mix, custom IDT Ultramer primers).

Then, 336 ng of each amplified library was processed with the Arbor Biosciences myBaits Mito kit, following manufacturer's instructions (manual version 4.01) and using their biotinylated bait panel specifically designed against the C. elegans mitochondrial genome. The enriched product was then PCR amplified for 11 additional cycles using universal p5 and p7 primers that anneal upstream of the multiplexing indices (NEBNext Ultra II Q5

Master Mix). Amplified libraries were separated and imaged on an Agilent TapeStation 2200 (High Sensitivity D1000 reagents) for quality control, and 80 nmol of each library was pooled for sequencing. The pooled library molecules had an average length of 369 bps.

Total-cellular shotgun libraries to control for NUMT derived mapping artifacts

Rare variant detection in mitochondrial genomes is complicated by the fact that mitochondrial sequences can occasionally be transferred to the nuclear genome (Richly and Leister 2004). These mitochondrial-derived nuclear genome sequences (referred to as NUMTs) accumulate point mutations as they are largely nonfunctional. NUMT-derived library fragments can map to the mitochondrial genome, and variants that have accumulated in NUMTs can be difficult to distinguish from true mitochondrial mutations (Hazkani-Covo et al. 2010). To overcome this challenge, we have previously implemented a k-mer count-based approach (Wu et al. 2020; Broz et al. 2021; Waneka et al. 2021), where counts of each putative mtDNA mutation are tabulated from a total-cellular shotgun DNA library. NUMT-derived variants are expected to have k-mer counts in the shotgun library that are similar to the counts for rest of the nuclear genome. In contrast, true mtDNA mutations are expected to have k-mer counts substantially lower (typically 0, barring sequencing errors and/or rare convergent mutations in the shotgun library) than the rest of the nuclear genome. We generated three replicate shotgun libraries for this purpose from total-cellular C. elegans DNA, following the same design used to generate the Duplex Sequencing replicates (Supplementary Figure S1). Three sibling nematodes were used to initiate lineages that were propagated for three generations before nematodes from several plates (per replicate) were pooled for DNA extraction. To limit the potential contribution of shared, heteroplasmic variants in our nine replicates and the shotgun samples, the parent of the three replicates was selected from a lineage of N2 nematodes divergent from the nine replicates we assay for mtDNA mutations. DNA was extracted using the Qiagen DNA Blood and Tissue Kit following manufacturer's instructions, and shotgun libraries were created using the NEBNext Ultra II FS DNA Library Prep Kit, with 50 ng of input DNA, a 15-minute fragmentation step, and 5 cycles of PCR amplification. Assessment of the shotgun libraries on the Agilent TapeStation 2200 (High Sensitivity D1000 reagents) revealed adaptor dimers, which were subsequently removed with size selection on a 2% BluePippin gel (Sage Science) using a target range of 300-700 bp. The resultant pooled sample had an average fragment length of 392 bp.

Sequencing of shotgun and Duplex Sequencing libraries, variant detection and analysis

Total-cellular shotgun libraries were sequenced on an Illumina NovaSeq 6000 platform (2 x 150 bp reads) at the University of Colorado Cancer Center, resulting in 18.1–22.2 M read pairs per library, equating to roughly 60× coverage of the C. elegans nuclear genome. The Duplex Sequencing libraries were sequenced on an Illumina HiSeq4000 platform (2 × 150 bp reads) by Novogene in two runs, resulting in a total of 66.8–76.9 M read pairs per library.

Duplex Sequencing reads were processed with our previously described pipeline (https://github.com/dbsloan/duplexseq; Wu et al. 2020), which (1) trims adaptor sequences (cutadapt v1.16; Martin 2011), (2) calls duplex consensus sequences (DCSs) based on shared random barcodes (each DCS required a minimum of six raw Illumina reads—at least three from each strand),

(3) filters out discordant DCSs with ambiguous bases resulting from disagreement between strands, (4) aligns concordant DCSs to the reference genome (NCBI reference sequence NC_001328.1; bowtie2 v2.3.5; Langmead and Salzberg 2012), (5) calls variants and DCS coverage by parsing the DCS alignment, and (6) filters NUMTS through a comparison to a k-mer database generated from the shotgun libraries (KMC v 3.0.0; https://github.com/re fresh-bio/KMC). An expected AT equilibrium was calculated as:

Frequency (AT decreasing subs) Freq(AT decreasing subs) + Freq(AT increasing subs)

To account for the nested structure of our data (i.e., replicates a, b, and c are nested within each population 1, 2, and 3), we implemented mixed linear models in R (ver 1.3.959), using the lme4 package. In such analyses, the genomic comparison of interest (e.g., substitution class or genome region) was set as a fixed effect, and replicate was set as a random effect nested within population, which was also set as a random effect.

Data availability

The raw reads are available via the NCBI Sequence Read Archive (SRA) under accessions SRR14352240-14352248 (Duplex Sequencing libraries; Supplementary Table S1) and SRR14352249, SRR14352237, and SRR14352238 (shotgun libraries 1, 2, and 3, respectively). The code used to process the raw reads, create consensus sequences, and call variants are available here: https:// github.com/dbsloan/duplexseq. The variants we detected through Duplex Sequencing are reported in Supplementary File S1 (SNVs) and Supplementary File S2 (indels). Supplementary material is available at figshare: https://doi.org/10.25386/genetics.14525493.

Results and discussion

Targeted Duplex Sequencing provides a highresolution view of mutation in the C. elegans mitochondrial genome

We enriched for mtDNA derived sequences through hybrid capture, which was highly effective, as 99.91% of all DCSs mapped to the C. elegans mitochondrial genome (each DCS is a consensus sequence produced from at least 6 concordant Illumina reads). In contrast, in a preliminary trial with Duplex Sequencing libraries made from total cellular C. elegans DNA (SRR14352239), less than 0.5% of DCSs mapped to the mitochondrial genome. For each of the nine replicates assayed, the average DCS coverage of the mitochondrial genome was 13,257×, with a range from 9099× in replicate 1b to 15,451× in replicate 1a (Supplementary Table S1).

We identified a total of 456 DCSs with SNVs and 17,582 DCSs with indels (SNVs: Supplementary File S1, indels: Supplementary File S2). These counts do not include one variant identified as a NUMT artifact based on k-mer counts in total-cellular shotgun libraries. The putative NUMT was present at a low frequency in every replicate and mapped to the only NUMT to have been previously identified in the C. elegans nuclear genome (Frith 2011). The above counts were tabulated after correcting three positions with fixed or nearly fixed differences in the nine replicates (Supplementary Table S2), which presumably represent existing differences in our N2 line compared to the published N2 mitochondrial genome (NC_001328.1). Raw DCS counts are inflated however by several variants present at high enough frequency to be detected in numerous DCSs. For example, a CG→TA

mutation at position 5079 was present at a frequency of 0.004 in replicate 1c (158 DCSs). Similarly, a 1-bp A insertion at position 3235 was present at a frequency above 0.5 in the population 2 replicates (15,317 DCSs). In total, 97.5% of DCSs with indels from the nine replicates mapped to position 3235 (17,158 DCSs; Supplementary File S2). Across all replicates, there were 235 unique sites with an SNV, 36 unique sites with an insertion, and 65 unique sites with a deletion. Although most SNVs were "singletons" detected in only one DCS, we did identify 23 SNVs that were represented by multiple DCSs from the same replicate.

The passage of the three populations (1, 2, and 3) through 10 individuals for 15 generations was intended to give heteroplasmic variants present in the ancestor of the populations a chance to reach different frequencies via selection or drift. If an ancestral variant was maintained in all three populations over the course of these 15 generations, we expected it to be present in all nine replicates, with variant frequencies within each population reflecting the variant frequency in the replicate founder (Supplementary Figure S1). Indeed, we found the insertion at position 3235 was present in all nine replicates. Furthermore, it was present at a frequency of 0.52–0.64 in the population 2 replicates, 0.054-0.098 in the population 1 replicates, and 0.00013-0.00079 in the population 3 replicates, suggesting that it had reached a frequency above 0.5 in the population 2 founder but was less common in the population 1 founder and was relatively rare in the population 3 founder. In contrast to this insertion, we found no SNVs were present in all 9 replicates. The highest amount of SNV sharing was a CG>TA substitution at position 5079, found in 4 replicates (1a, 1c, 2a, and 3c).

Given that the 15 generations of private segregation provided an opportunity for new variants to arise, we expected to find that some variants would be exclusively shared among replicates from a population. However, we did not find any indels or SNVs that were exclusively shared among replicates from the same population (Supplementary Files S1 and S2). This suggests that the majority of mutations we detected occurred during replicate expansion (Supplementary Figure S1). This idea is supported by the observation that the majority of SNVs (230 of 253) were singletons detected in only a one DCS (Supplementary File S1), suggesting they are rare within the replicates. In the 18 instances where SNVs were shared among replicates, those replicates almost always belonged to different populations (e.g., 2a and 3c), with the exception of the aforementioned CG→TA substitution at position 5079, as well as a AT→GC substitution at position 8999, which was present in replicates 1b, 1c, and 2c. Given that the majority of shared SNVs are shared across populations, we posit that most shared SNVs arose through independent mutations and for downstream analyses we interpreted shared mutations as independent counts, resulting in 253 SNVs. While this is the most parsimonious interpretation, we cannot rule out the possibility that shared SNVs are ancestral events that were independently lost in the majority of the replicates. Such an interpretation yields slightly decreased counts of 235 SNVs. Importantly, these counts yield a nearly identical mutation spectrum (see Supplementary Figure S2 and Supplementary Table S3) to the one presented below, demonstrating that our findings are robust regardless of the interpretation of shared SNVs as ancestral or independent events.

The 253 SNVs include six sites which were tri-allelic. In all six cases, a CG reference base-pair experienced both a CG→TA transition and a CG-AT transversion. Three of these six sites were tri-allelic within a single replicate. We observed only a single dinucleotide substitution: an AA→GG change at position 5010 in

replicate 1c. The count of 445 total mutations (253 SNVs plus 192 indels) observed here is ninefold higher than the highest count (51 mutations; Howe et al. 2010) detected in any nematode MA experiment to date (Denver et al. 2000; Molnar et al. 2011; Konrad et al. 2017; Wagner et al. 2020). Although this bulked sequencing approach of whole nematode populations is not conducive to estimating an absolute mutation rate per generation, the large number of detected variants makes it a powerful one for characterizing the spectrum and distribution of mutations.

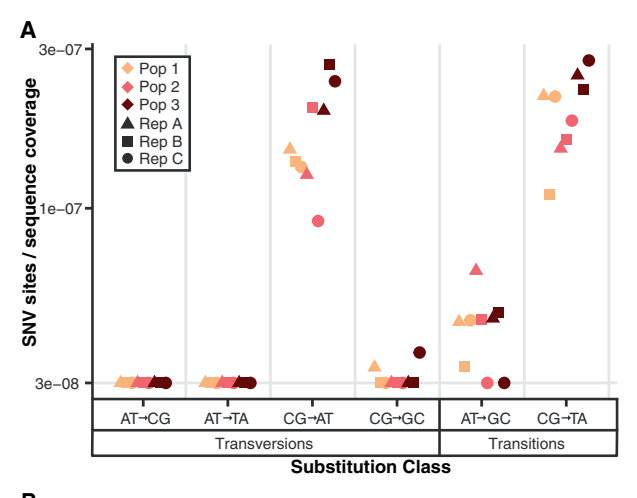
Low-frequency variants detected in C. elegans mtDNA indicate a strong bias towards mutations that increase AT content

We found significant variation in the (log transformed) SNV frequency between the six substitution classes (one-way ANOVA, $P \ll 0.0001$; Figure 1A). CG \rightarrow TA transition and CG \rightarrow AT transversion frequencies were similar to one another (2.09×10^{-7}) and 1.81×10^{-7} , respectively), and 3- to 16-fold higher than the frequencies in the other substitution classes. Previous MA experiments to analyze nematode mtDNA mutation spectra have also reported a dominance of CG-TA transitions (Howe et al. 2010; Konrad et al. 2017), but only one C. briggsae study (with a count of 10 total SNVs), reported CG→AT transversions at a similar relative abundance to CG→TA transitions (Wagner et al. 2020).

We asked if the C. elegans mtDNA is at AT equilibrium, in which case the number of AT-decreasing mutations would equal the number of AT-increasing mutations. Given the dominance of CG→TA transitions and CG→AT transversions in the spectrum (Figure 1A), it was not surprising that the AT-increasing count of 173 was significantly greater than the AT-decreasing count of 52 (binomial test, $P \ll 0.0001$). This difference is not driven by differences in AT vs GC sequencing coverage, as the coverage-adjusted AT-decreasing count (normalized by the ratio of AT coverage per base pair over GC coverage per base pair, as in Waneka et al. 2021) of 61 was still significantly less than the adjusted AT-increasing count of 164 (binomial test, $P \ll 0.0001$). We used the coverageadjusted counts to determine an expected AT equilibrium of 89.4% (formula in Methods). This expected value is substantially larger than the actual mtDNA AT content (75.6%), slightly greater than the AT content at fourfold degenerate sites (86.4%), and slightly less than AT content of the two intergenic regions of the C. elegans mtDNA (90.8% AT). These results suggest that AT mutation bias would push the C. elegans mtDNA to even more extreme AT contents if not for the stabilizing effects of natural selection, thus supporting the findings of Konrad et al. (2017) which ran contrary to the earlier report of a mutational bias towards GC in C. elegans mtDNA (Denver et al. 2000).

Asymmetries between forward and reverse mtDNA strands suggest differences in singlestranded damage

Several biological processes, including replication (Kennedy et al. 2013) and transcription (Liu and Zhang 2020), can lead to systematic differences in the amount of DNA damage experienced by the two DNA strands. By definition, mutations affect both strands of DNA, but single-stranded asymmetries can be studied by comparing the frequency of reciprocal single-stranded changes for each substitution class (e.g., $C \rightarrow T$ vs. $G \rightarrow A$ changes) on a given DNA strand. The coding sequence for all of C. elegans mtDNA genes (12 protein-coding genes, the two rRNA genes, and the 22 tRNA genes) are oriented in the same direction on one DNA strand (hereafter F-strand for forward strand) (Okimoto et al. 1992). To search for signatures of DNA damage in our Duplex



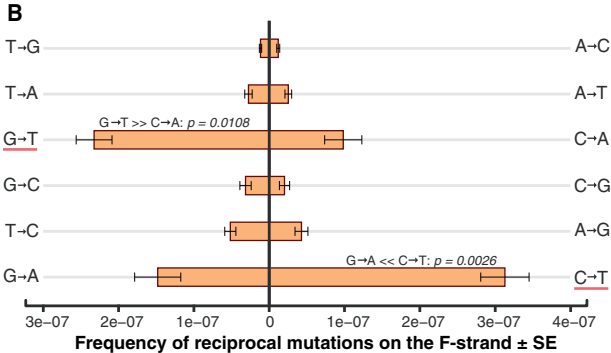


Figure 1 The C. elegans mtDNA mutation spectrum is dominated by mutations that increase AT content and exhibits strand asymmetry. (A) Variation in the frequency of mutations across six substitution classes. CG→AT transversions and CG→TA transitions are the most abundant substitution types. Each point on the plot represents one of the nine replicates assayed. SNV frequencies were calculated as the number of sites in a replicate with a mutation normalized by the coverage of the corresponding base pair type. For example, the CG→AT mutation frequency shows the CG→AT event count divided by GC coverage for each replicate. A floor was applied to frequencies below 3e-08, which approaches the error threshold of Duplex Sequencing (Wu et al. 2020). (B) Strand asymmetry of mutations in C. elegans mtDNA. Both CG→AT and CG-TA substitutions show significant strand asymmetry (one-way ANOVA, P-values noted on figure), with the $G \rightarrow T$ and $C \rightarrow T$ changes (underlined in red) occurring predominately on the forward (F) strand, which in C. elegans mtDNA is synonymous with the heavy-strand and for genic regions also the coding-strand. Mutation frequencies were calculated as the average of the nine replicates and were normalized by the sequencing coverage of each base type on the F-strand. For example, the $G \rightarrow T$ mutation frequency shows all $G \rightarrow T$ events on the F-strand divided by G coverage on the F-strand, and the C→A mutation frequency shows all C→A events on the F-strand divided by C coverage on the F-

Sequencing data, we performed a strand asymmetry test for each of the six substitution classes. This analysis revealed significant asymmetries in both CG→TA transitions and CG→AT transversions (one-way ANOVAs, P = 0.0026 and 0.0108, respectively), with disproportionate amounts of $C \rightarrow T$ and $G \rightarrow T$ changes occurring on the F-strand (Figure 1B).

The role of oxidative damage in the C. elegans mtDNA mutation spectrum and strand asymmetries

CG→AT transversions are indicative of oxidative damage because oxidized guanines (e.g., 8-oxo-G) are often mis-paired with adenine, causing $G \rightarrow T$ changes (Kennedy et al. 2013; Kino et al. 2017). The relative abundance of CG→AT transversions in the *C. elegans* mtDNA Duplex Sequencing spectrum (Figure 1A) compared to mtDNA mutation spectra produced through high-fidelity sequencing in other metazoans (Kennedy et al. 2013; Itsara et al. 2014; Ni et al. 2015; Samstag et al. 2018; Arbeithuber et al. 2020) suggests that oxidative damage may be particularly important for driving mtDNA mutation in nematodes. The 2.3-fold enrichment of G→T changes on the F-strand (Figure 1B) provides evidence that the abundance of CG-AT transversions observed here is not artifactual and suggests the F-strand suffers increased loads of oxidative damage in vivo. The other common substitution class in our data, CG→TA transitions, are likely also driven by strand-specific damage (cytosine deamination), given the 2.1fold enrichment of C→T changes on the F-strand. Cytosine deamination can be related to oxidative damage, but it can also occur spontaneously via hydrolysis in the absence of oxidative damage (Kreutzer and Essigmann 1998; Nabel et al. 2012).

Previous high-fidelity sequencing studies observing $C \rightarrow T$ vs G→A strand asymmetries in mtDNAs of fruit flies (Itsara et al. 2014), mice (Arbeithuber et al. 2020), and humans (Kennedy et al. 2013) have hypothesized that increased spontaneous deamination of cytosine on the F-strand (referred to as the H-strand or minor-strand in those systems) occurs due to increased singlestranded exposure during mtDNA replication (Falkenberg 2018). C. elegans mtDNA replication is distinct from the stranddisplacement or strand-coupled mtDNA replication models which have been characterized in vertebrates and insects (Yasukawa et al. 2006; Jõers and Jacobs 2013; Cluett et al. 2018; Falkenberg 2018). In C. elegans, mtDNAs are replicated through a rolling circle mechanism which produces double-stranded concatemers up to 48.2 kb in length $(3.5 \times \text{ the length of a single mtDNA})$ Lewis et al. 2015). In characterizing the rolling circle mechanism of mtDNA replication utilized by C. elegans, Lewis et al. (2015) found some evidence of single-stranded DNA through transmission electron microscopy but noted that "replication intermediates lack the extensive single-stranded DNA character expected from strand-displacement synthesis." Interestingly, the magnitudes of the asymmetries observed here (2.3-fold for $G \rightarrow T$ changes and 2.1-fold for C→T changes on the F-strand) are substantially lower than the $C\rightarrow T$ enrichment on equivalent strands in aged mice (7.9- to 11.9-fold depending on the tissue-type; Arbeithuber et al. 2020), humans (Kennedy et al. 2013), and fruit flies (Itsara et al. 2014). In the latter two studies, the magnitudes of strand asymmetries were not reported explicitly but were >10fold based on study data. We posit that the reduced magnitude of strand asymmetries in C. elegans may be associated with the lack of single-stranded intermediates reported by Lewis et. al. (2015). Transcription may also drive mutational asymmetries observed here, as the coding (or sense) strand may be exposed while RNA polymerases bind and read off of the template strand (Liu and Zhang 2020). Because the template sequences for all C. elegans mtDNA genes are located on the same strand, it is unclear if the F-strand suffers increased single-stranded exposure due to replication, transcription or both.

Interestingly, rolling circle replication can apparently be induced in mtDNAs of human cells through treatment with H₂O₂ (a ROS; Ling et al. 2016; Ling and Yoshida 2020), indirectly supporting the link between rolling circle replication and oxidative stress in C. elegans mtDNAs. Assays with human Pol γ in vitro reveal the polymerase is particularly prone to misincorporations leading to AT→GC and CG→TA transitions (Longley et al. 2001; Zheng et al. 2006). Misincorporations by the nematode Pol γ have not been characterized, so it is possible that the relative

abundance of CG-AT transversions in the Duplex Sequencing spectrum could reflect distinct replication errors of the C. elegans Pol γ. However, such polymerase error would be unable to explain the $G \rightarrow T$ vs $C \rightarrow A$ strand asymmetries that we observed (Figure

In metazoan mtDNAs, BER of oxidized guanines is hypothesized to be mediated by mitochondrially targeted glycosylases OGG1 and/or MUTYH. However, ogg1 mutant flies (Itsara et al. 2014) and ogg1/mutyh double mutant mice (Kauppila et al. 2018) show no increase in mtDNA mutations compared to wild-type individuals, even when mitochondria ROS levels are elevated through knockout of the mitochondrially targeted superoxide dismutase (Sod2) in these lines. Interestingly, C. elegans lines lacking mitochondrially targeted SODs experience significantly elevated mtDNA damage compared to wild-type lines, as measured with short- and long-amplicon quantitative real-time PCR (Ng et al. 2019). mtDNA mutations have not yet been assessed in C. elegans sod mutants or in lines with deficiencies in BER. While the relative abundance of CG-AT transversions in our Duplex Sequencing data supports a role of oxidative damage in driving C. elegans mtDNA mutations, we do not consider this evidence in support of the mitochondrial free radical theory of aging (mFRTA). The mFRTA posits that oxidative stress is causal to aging (Harman 1972). While we find evidence that oxidative stress may be causal to mtDNA mutations in C. elegans, previous studies which have more explicitly tested the mFRTA in C. elegans have not found a consistent link between oxidative stress and nematode lifespan (Van Raamsdonk and Hekimi 2009; Gruber et al. 2011; Ng et al.

Comparisons to other mtDNA mutation studies

It is unlikely that the relative abundance of CG→AT transversions reported here is an artifact of Duplex Sequencing because we have recovered a diversity of unique mutation spectra with this same technique in various other biological systems (Wu et al. 2020; Broz et al. 2021; Waneka et al. 2021), some of which have shown very low relative frequencies of CG-AT transversions. Furthermore, Duplex Sequencing, when used to measure mutations in human and mice mtDNAs, yielded spectra with very few CG→AT transversions (Kennedy et al. 2013 and Arbeithuber et al. 2020, respectively). Different high fidelity techniques have also revealed spectra relatively deplete of CG-AT transversions in the mtDNAs of wild-type fruit flies (Itsara et al. 2014) and mice (Ni et al. 2015).

Given that we detected mutations in pooled somatic and germline tissues, we considered the possibility that the relative abundance of CG→AT transversions in the Duplex Sequencing spectrum (Figure 1A) compared to what has been reported in nematode MA studies (Howe et al. 2010; Molnar et al. 2011; Konrad et al. 2017) could reflect distinct mutational spectra in somatic vs. germline mtDNAs. Such a distinction would imply that oxidative damage and associated CG→AT transversions are more prevalent in somatic mtDNAs than in the mtDNAs maintained in the nematode germline. The mixed-stage populations from which we extracted DNA likely included some older individuals (no older than 14–16 days old, the total time of replicate growth; Supplementary Figure S1), potentially increasing the contribution of somatic mtDNA mutations (Kennedy et al. 2013; Arbeithuber et al. 2020). However, studies of mtDNA replication across C. elegans development in mutant lines with deficiencies in Pol γ have established that mtDNA replication occurs primarily in the nematode gonad, such that essentially all somatic mtDNAs originate at embryogenesis (Bratic et al. 2009). The embryonic origin of somatic mtDNAs therefore blurs the distinction between somatic and germline mtDNAs in nematodes. If the abundance of CG-AT transversions is caused by oxidative damage to mtDNA in somatic tissues, it would indicate that there is some degree of active mtDNA replication or erroneous mtDNA repair converting single-stranded DNA damage into double-stranded mutations detectable with Duplex Sequencing. Given that our mitochondrial DCS coverage (13,257× on average) is well below the estimated number of nematodes in each tissue pool (~50,000 assuming each of the 10 plates pooled for each replicate contained ~5000 nematodes), we have likely sampled less than one mtDNA per nematode. Therefore, the 23 mutations that were detected in >1DCS in our dataset are more likely to be inherited, germline mtDNA mutations, present in multiple individuals within a replicate. Importantly, these sites yielded a spectrum with a similar frequency of CG→AT transversions (35% of all substitutions; Supplementary Table S4) as in the full dataset (32% of all substitutions; Supplementary Table S4; Figure 1A). Still, it is possible that the spectrum reported here is influenced in part by distinct mutational patterns in somatic mtDNAs.

Differences in our culturing protocol compared to those used in MA studies could also explain differences in mutation spectra. We reared our nematodes on identical media (NGM) to what has been used in MA experiments (Denver et al. 2000; Konrad et al. 2017), but our final cultures had a much higher density compared to the low number of nematodes maintained in MA experiments. Though we monitored our cultures daily to ensure food availability, we cannot rule out the possibility that our cultures could have experienced increased stress associated with crowding compared to the cultures maintained in MA experiments.

Another potential explanation for the differences in the Duplex Sequencing results compared to those from MA studies is that our spectrum consists mostly of extremely rare variants captured by only a single DCS (230 of 253 observed SNVs), whereas nematode MA studies have applied detection cutoffs requiring variants to be present in at least 3 or 4 unique reads (for Illumina based studies with coverages of approximately 388 or 282; Konrad et al. 2017 and Wagner et al. 2020, respectively) or simply as "detectable on a chromatogram" for Sanger based studies (Denver et al. 2000; Howe et al. 2010; Molnar et al. 2011). Given that the mutations detected in MA studies were initially generated as only a single copy within an individual and had to rise in frequency to meet detection thresholds, it seems likely that the MA mutation spectra could be biased by selection. Even small selective biases may have dramatic effects on observed spectra given that C. elegans MA studies passaged lineages for 214 or 363 generations (roughly two or three years of propagation; Denver et al. 2000 and Konrad et al. 2017, respectively), whereas our culturing design allowed just three generations for mutations to occur (Supplementary Figure S1). By minimizing the number of generations, we may have reduced the opportunity for within-individual selection to shape the mutation spectrum, although this trades off with the fact that the absence of the bottlenecking used in MA lines would allow for selection to act at an organismal level in these three generations.

If CG→AT transversions experience stronger negative selection than CG→TA transitions, which is plausible since transversions are more likely to result in amino acid changes (Okimoto et al. 1992), they could be underrepresented in MA studies due to within-individual selection pressures. Indeed, in our Duplex Sequencing Data 93.4% (57/61) of CG→AT transversions but only 75.6% (61/82) of CG→TA transitions result in amino acid changes (Supplementary File S1). This same logic has been used to explain

an underrepresentation of nuclear CG→AT transversions in natural nematode populations compared to the relative abundance of nuclear CG→AT transversions in multiple nematode MA studies (Denver et al. 2012; Weller et al. 2014) because in that comparison, the natural population spectrum is expected to be more strongly affected by selection (Rajaei et al. 2021). Konrad et al (2017) compared C. elegans mtDNAs from 38 natural isolates (sequenced in Thompson et al. 2013) and found that transitions (including both CG→TA and TA→CG changes, which cannot be reliably polarized in the population dataset) account for 83% of the 408 observed substitutions, yielding a transition/transversion ratio (hereafter Ti/Tv ratio) of 4.75 (Supplementary Table S5). The dominance of transitions at the population level appears to be driven in part by stronger selection against transversions because constraining the population data set to the 162 substitutions at fourfold degenerate sites yields a reduced Ti/Tv ratio of 3.26 (Supplementary Table S5). The fourfold degenerate Ti/Tv ratio is still substantially higher than the Ti/Tv ratio we observe with Duplex Sequencing (1.32; Supplementary Table S5). Considering that fourfold degenerate sites are expected to experience minimal selection, the elevated Ti/Tv ratio at fourfold sites compared to the one from our Duplex Sequencing data suggests the latter may not be fully representative of inherited mtDNA mutations in natural C. elegans populations.

Distribution of mtDNA SNVs across the mitochondrial genome.

The large number of SNVs we detected with Duplex Sequencing allowed us to study how these events are distributed across the genome. As shown in the middle track (red histogram) of Figure 2A, the depth of DCS coverage varied substantially across the genome. Much of this variation can likely be attributed to differences in local GC content, as the AT DCS coverage (summed across replicates) accounted for only 72.1% of all DCS coverage, despite the fact that the mitochondrial genome is 75.6% AT. The AT vs. GC coverage disparity is exaggerated in regions with long stretches of sequence that are AT rich, as the 10% of 50 bp windows with the lowest GC content have 8.9-fold lower DCS coverage than windows of median GC content, and 17.5-fold lower DCS coverage than the 10% windows with the highest GC content (Supplementary Figure S3). Still, 95.6% of 50-bp windows had DCS coverage (summed across nine replicates) above 1000×. Bias against AT-rich sequences during library amplification and decreased binding affinities for AT rich baits during mtDNA enrichment both likely contribute to decreased AT coverage.

After correcting for differences in coverage, we found no variation in mutation frequency between intergenic regions, proteincoding genes, rRNA genes, or tRNA genes (one-way ANOVA, P=0.99; Figure 2B). However, comparisons against intergenic sequences are low powered given the relative lack of intergenic coverage (the largest of the two noncoding regions is extremely AT rich: 465 bp, 93.3% AT). A previous Duplex Sequencing study also found no variation across intergenic regions, protein-coding genes, rRNA genes or tRNA genes in both wildtype fruit flies and in lines with a proofreading-deficient Pol γ (Samstag et al. 2018). We then tested for differences in mutation rates among proteincoding genes, which comprise 74.5% of the C. elegans mtDNA. We found significant variation (one-way ANOVA, P = 0.0072; Supplementary Figure S4) driven by between-gene differences in CG-TA transition and CG-AT transversion frequencies (oneway ANOVAs, P = 0.016 and 6.3×10^{-5} , respectively; Figure 2C).

The cause of differences in SNV frequencies between genes remains unclear. Given the aforementioned mutational bias

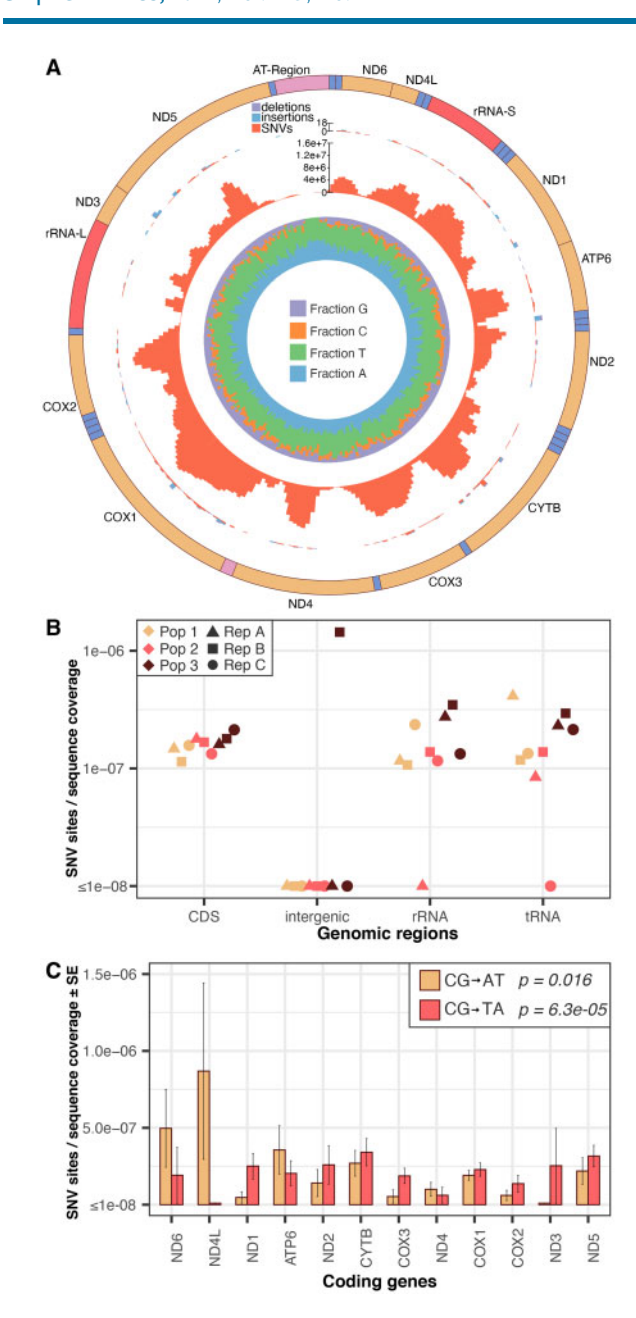


Figure 2 The distribution of mutations across the mitochondrial genome. (A) Map of the C. elegans mtDNA and summary of Duplex Sequencing data. The outermost track depicts the gene order and type, with protein-coding (CDS) genes shown in tan, rRNA genes shown in red, tRNA genes shown in blue, and intergenic regions shown in pink. The next track in from the outside depicts the total mutation counts in 50-bp windows, with deletions, insertions and SNVs colored differently according to the key at the top of the track. The next track in from the outside (red histogram) depicts the cumulative (sum of nine replicates) DCS coverage in 50-bp windows, with a scale bar included at the top of the track. The innermost track shows the relative fraction of each base type in 50-bp windows, with colors specified by the key in the figure center. The figure was generated with Circos v0.69-8 (Krzywinski et al. 2009). (B) Variation in SNV frequencies by genomic region. Note that low intergenic coverage resulted in the detection of only a single intergenic substitution (in replicate 3b). The other replicates had intergenic substitution counts of zero, but also had extremely low intergenic coverage, making comparisons that include intergenic SNV frequency low powered (see main text). No significant variation is observed among CDS, tRNA, or rRNA genes when the intergenic region is excluded. (C) Significant variation in SNV frequencies across the 12 protein-coding genes was observed for only the two most common substitution classes (CG→AT transversions and CG→TA transitions). See Supplementary Figure S4 for the gene specific mutation frequencies of all substitution classes.

away from GC base pairs, we considered if differences in GC content among genes could be driving differences in SNV frequencies. There is a weak, positive correlation between gene-wide GC content and gene specific CG-TA transition frequencies (Pearson correlation: r = 0.32, P = 0.304; Supplementary Figure S5) and a negative correlation between GC content and gene specific CG \rightarrow TA transversion frequencies (Pearson correlation: r=-0.51, P=0.086; Supplementary Figure S5), but neither was significant. Therefore, GC content variation does not explain differences in gene-specific mutation frequencies.

CG→TA transitions and CG→AT transversions both also show significant strand asymmetries (Figure 1B), so it seems possible that distance from an origin of replication (Kono et al. 2018) or differential transcription (Gaillard and Aguilera 2016; Wang et al. 2016) could play a role in driving mutation rate differences among genes (Figure 2C). To investigate this possibility, we plotted the $C \rightarrow T$ and $G \rightarrow T$ enrichment values along the distance of the mitochondrial chromosome in 1000-bp sliding windows, with a step size of 100 bp (Supplementary Figure S6). This analysis is low powered since a relatively small number of mutations (94 CG→TA transitions and 79 CG→AT transversions) are split over 275 windows, but it appears that for both substitution types, the N→T enrichment is highest near the beginning of the chromosome and slopes downward over the duration of the chromosome (Supplementary Figure S6). This result is consistent with the observation that C→T enrichment slopes away from the control region (heavy-strand origin of replication) in mice and human mtDNAs (Sanchez-Contreras et al. 2021). In C. elegans, the intergenic region upstream of ND6 (labeled "AT region" and drawn in pink in Figure 2A) contains short repetitive elements which led several to propose this region may be analogous to the control region in mammalian mtDNAs, acting as the F-strand replication origin (Lemire 2005; Bratic et al. 2010). However, this region lacks a GC skew inflection point typical of replication origins (Kono et al. 2018) and fails to form bubble arcs indicative of replication origins in two-dimensional gel electrophoreses (Lewis et al. 2015). Our finding that N→T enrichment values slope away from the AT-region in C. elegans suggests that the sequence downstream of the AT-region may experience increased time in a single-stranded state, which is expected under a strand-displacement model of mtDNA replication (Sanchez-Contreras et al. 2021). As noted however, our analysis of asymmetry across the chromosome is low powered, so we interpret this finding cautiously.

It is unlikely that differences in expression drive among gene mutation rate differences, as the C. elegans mtDNA is likely transcribed as a polycistronic RNA (Blumberg et al. 2017), with differences in relative abundances of specific mRNA transcripts presumed to arise from differences in mRNA stability and decay (D'Souza and Minczuk 2018). Reverse-transcriptase droplet digital PCR (ddPCR) estimates reveal relatively small differences (~9-fold) in mRNAs levels among protein-coding genes in the C. elegans mitochondria, while rRNAs are 50- to 200-fold more abundant than mRNAs (Held and Patel 2020). If transcription does drive mutation C. elegans mtDNAs, our finding of no difference in mutation rates between rRNA coding genes and protein-coding genes (Figure 2B) supports the hypothesis that different levels of rRNA vs. mRNA arise through increased rRNA stability or mRNA decay (Held and Patel 2020). Yet another possibility, discussed below, is that differences in mutation frequencies among genes could be driven by local sequence features that are correlated with mutation and vary among genes.

Distribution of mtDNA SNVs based on local sequence variation.

Previous analyses of mtDNA mutations in flies (Samstag et al. 2018) and mice (Ni et al. 2015) have shown that the identities of neighboring nucleotides can have large impacts on mtDNA mutation frequencies. To understand if local sequence contexts influence SNV frequencies in the C. elegans mtDNA, we compared the variant frequencies at the 16 trinucleotide contexts (i.e., the mutated site and the flanking 5' and 3' nucleotides) for each substitution class and found significant effects for both CG-TA transitions and CG-AT transversions (one-way ANOVAs, P = 0.040 and 3.6×10^{-5} , respectively), but not in any of the other substitution classes (Figure 3). It is likely that CG→TA transitions and CG→AT transversions are the only substitution types to show significant trinucleotide variation because they make up the majority of detected SNVs, while tests for variation in the other substitution classes are comparatively low powered. Different trinucleotides are apparently important in the two significant substitution classes. CG

TA transitions are particularly common at GCC/GGC, GCG/CGC, and CCC/GGG trinucleotides (written 5' to 3'). In contrast, CG→AT transversions are particularly common at ACT/AGT and ACG/CGT trinucleotides. It is possible that the above reported genic mutation rate variation among protein-coding genes (Figure 2C) may be driven by a nonrandom distribution of "mutagenic" trinucleotides.

Nonsynonymous mutations are slightly more abundant than predicted by neutral simulations

To assess whether the identified sample of mutations was biased by selection, we used a simulation-based approach to obtain a

neutral expectation for the ratio of nonsynonymous to synonymous (NS: S) mutations. There were 205 observed SNVs in protein-coding sequences (Supplementary File S1), which we simulated onto a concatenation of the protein-coding sequence. We attempted to control for the C. elegans mutation spectra and probability of detection by simulating the same number and type of each substitution from our observed data. This simulation was repeated 10,000 times to obtain a distribution of NS: S ratios. Our observed NS: S ratio of 3.01 was 1.3-fold higher than the median simulated value of 2.23 (P = 0.075). This result suggests that neither synonymous nor nonsynonymous substitutions are significantly overrepresented in the observed Duplex Sequencing dataset (Figure 4). As such, there is no evidence that purifying selection has played a large role in filtering this pool of lowfrequency variants. Why the observed ratio contained a (marginally) higher proportion of nonsynonymous substitutions than the simulated ratio is not clear, though a previous study of mtDNA mutations in Drosophila melanogaster reported a significant overabundance of nonsynonymous substitutions compared to neutral expectations in a similar simulation-based test (Samstag et al. 2018). Those authors proposed that deleterious mutations may reduce mitochondrial function, thus reducing the potential for oxidative damage and by extension make mutant bearing mitochondria "less prone to targeted degradation by quality control surveillance" (Samstag et al. 2018).

Indels are predominantly expansions or contractions of existing homopolymers

The aforementioned C. elegans MA experiments reached different conclusions regarding the relative abundance of indels us SNVs

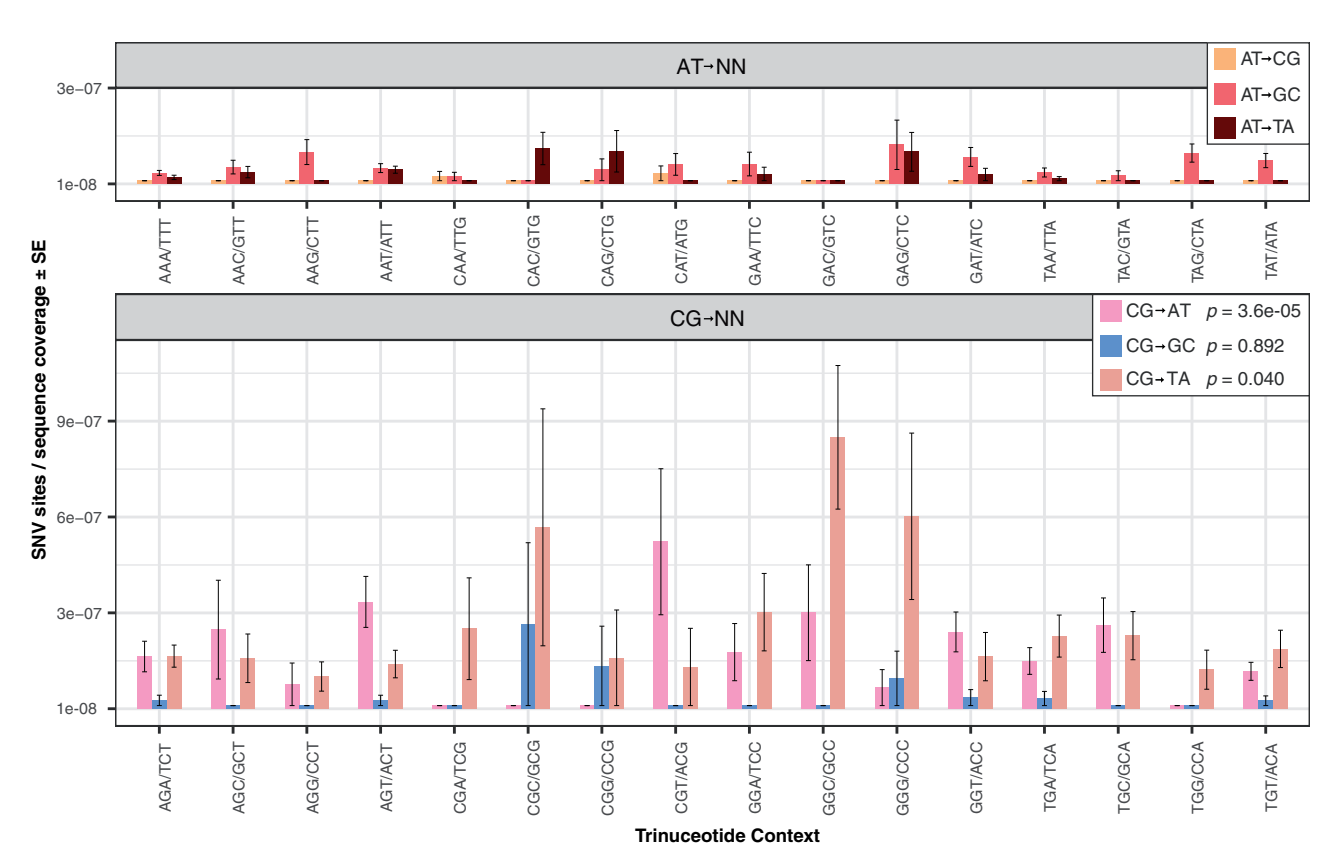


Figure 3 Variation in AT-NN (top panel) and CG-NN (bottom panel) mutation frequency across different trinucleotide contexts, where NN refers to any other base-pair. Significant variation was seen in the trinucleotide contexts for CG-AT transversions and CG-TA transitions (one-way ANOVA, P-values in figure legend).

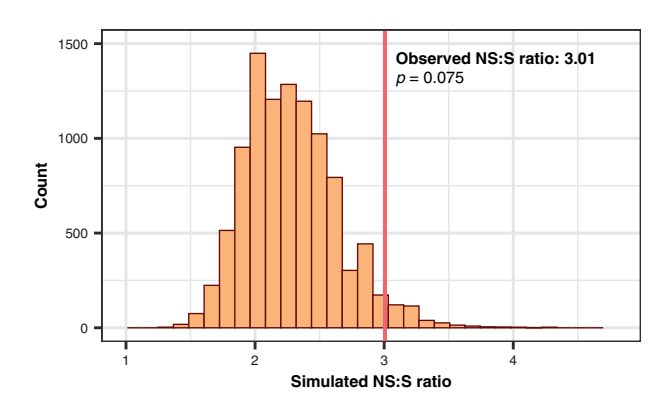


Figure 4 Simulation of mutations to derive null expectation of the ratio of nonsynonymous: synonymous substitutions (NS: S). The observed ratio of NS: S (marked with the vertical red line) is 1.3-fold higher than the null expectation generated from 10,000 simulations where the observed number and type of coding sequence mutations were randomly mapped onto the coding sequence, though this difference is not significant. The two-tailed P-value was derived by dividing twice the number of simulated NS: S ratios with values greater than the observed NS: S ratio by the total number of simulations (378*2/10000).

in mtDNAs, with the original study reporting an indel: SNV ratio of 0.65 (Denver et al. 2000) and the later study reporting a ratio of 1.42 (Konrad et al. 2017). As noted above, we found that many identical indels were shared across replicates and that numerous sites with indels had high variant allele frequencies, which could result either from a single mutation that rose in frequency, or multiple independent mutations at the same site. If indels are more prone to homoplasy within replicates (than SNVs), which may well be the case at long homopolymers (single-nucleotide repeats), this would lead us to underestimate the indel: SNV ratio. In addition, if multiple independent indels occur at different locations within the same homopolymer, both will map as an indel at the first site, since in our read mapping step all indels are left aligned. Furthermore, Duplex Sequencing coupled with hybridization-based enrichment is not designed to detect large deletions, which have been shown to accumulate at a high rate in mtDNAs of C. briggsae (Howe et al. 2010; Wagner et al. 2020). Given these concerns, we cautiously interpret our finding that indels are less common than SNVs in our data, a conclusion we reach whether shared mutations are assumed to be independent events (yielding an indel: SNV ratio of 0.75) or if they are assumed to be ancestral (yielding an indel: SNV ratio of 0.43).

We find different results for the relative abundance of insertions vs. deletions depending on how we categorize shared mutations. Deletions are about \sim 2-fold more abundant than insertions (65 vs 36, respectively) when we assume that shared mutations arose through common ancestry. However, when assuming shared indels are independent events that arise through homoplasy, we see a difference in the other direction (84 deletions vs 108 insertions). This discrepancy reflects the fact that identical insertions were more commonly shared between replicates than were identical deletions.

We surveyed the sequence surrounding each of the observed indels and found that the majority of both insertions and deletions are 1-bp expansions or contractions of existing homopolymers, which is consistent with previous C. elegans MA studies (Denver et al. 2000; Konrad et al. 2017). This pattern holds regardless of whether we assume shared indels arose through homoplasy (Figure 5) or common ancestry (Supplementary Figure S7). Because indels are left aligned in our read mapping step, we are unable to tell where in the homopolymer the indel occurred. The

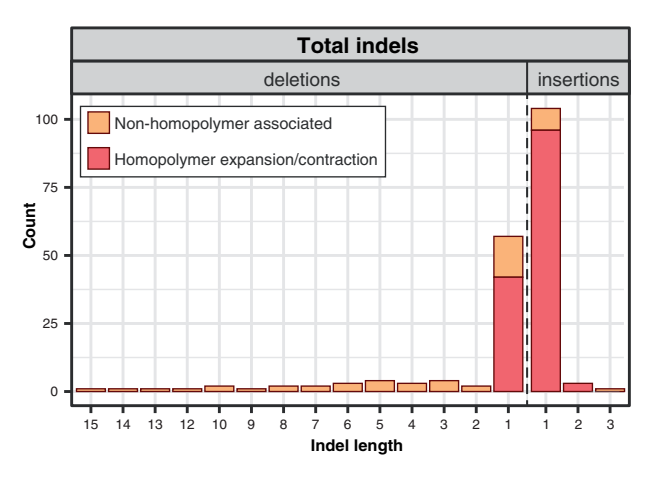


Figure 5 Indels are predominately found at homopolymers in C. elegans mtDNA. Here, indels that were shared between replicates were treated as independent events. See Supplementary Figure S5 for counts that assume indels shared between replicates are the result of common ancestry. Indels that are expansions or contractions of existing homopolymers are shown in red, while those that are not associated with homopolymers are shown in tan.

length of both insertions and deletions skews heavily towards 1bp mutations, especially for insertions, as we did not observe a single insertion above 3 bp. We found 22 deletions greater than 3 bp in length, with the largest being 15 bp in length. None of the deletions greater than 1 bp in length were associated with homopolymers.

Conclusions

Duplex Sequencing is a promising alternative approach to labor and time-intensive MA experiments for understanding mutational spectra and mechanisms of mutation in metazoan mtDNAs. The idea that these genomes experience increased mutational loads given the proximity of the mtDNA to electron transport and associated ROS (Harman 1972) predates initial observations that mtDNA mutation rates are elevated above nuclear mutation rates in metazoans (Brown et al. 1979). However, numerous experimental studies have not supported the hypothesis that oxidative damage drives rapid mtDNA evolution (Halsne et al. 2012; Kennedy et al. 2013; Itsara et al. 2014). The large number of variants we detected with Duplex Sequencing provide a high-resolution view of the C. elegans mtDNA mutation spectrum (Figure 1A). These data support a role for oxidative damage because one of the predominant mutation classes, CG→AT transversions, is considered to be a hallmark of oxidative damage (Kennedy et al. 2013; Kino et al. 2017; Krašovec et al. 2017; Poetsch et al. 2018). In addition to CG→AT transversions, the spectrum also contains a high frequency of CG→TA transitions, and both classes show significant strand asymmetries (Figure 1B), with C→T and G→T changes enriched on the F-strand, providing further support that C. elegans mtDNA mutations are driven by single-stranded DNA damage. In contrast, if CG→TA transitions and CG→AT transversions were prevalent as a consequence of Pol γ misincorporations, it is not clear how this would lead to the strand asymmetries observed here. Further investigation is warranted to understand why CG→AT transversions are so abundant in the mtDNA of C. elegans, but relatively deplete in other metazoan mtDNAs. A surprising finding from recent experiments in mice (Kauppila et al. 2018) and fruit flies is that CG→AT transversions remain rare even in animals with deficiencies in BER (the principal pathway for repair of damaged DNA). Considering the high rate of CG→AT transversions observed here, it would be interesting to repeat this study with C. elegans lines lacking BER capabilities.

Acknowledgments

The authors thank Tai Montgomery for supplying N2 nematodes, media, and laboratory space. They also thank Anne Hess for help in implementing the mixed linear models used in this study.

Funding

This work was supported by the National Institutes of Health (1R01GM118046 and 1R35GM142836) and a National Science Foundation graduate fellowship (DGE-1450032).

Conflicts of interest

None declared.

Literature cited

- Allio R, Donega S, Galtier N, Nabholz B. 2017. Large variation in the ratio of mitochondrial to nuclear mutation rate across animals: Implications for genetic diversity and the use of mitochondrial DNA as a molecular marker. Mol Biol Evol. 34:2762-2772.
- Anderson AP, Luo X, Russell W, Yin YW. 2020. Oxidative damage diminishes mitochondrial DNA polymerase replication fidelity. Nucleic Acids Res. 48:817-829.
- Arbeithuber B, Hester J, Cremona MA, Stoler N, Zaidi A, et al. 2020. Age-related accumulation of de novo mitochondrial mutations in mammalian oocytes and somatic tissues. PLoS Biol. 18:e3000745.
- Bernt M, Bleidorn C, Braband A, Dambach J, Donath A, et al. 2013. A comprehensive analysis of bilaterian mitochondrial genomes and phylogeny. Mol Phylogenet Evol. 69:352-364.
- Blumberg A, Rice EJ, Kundaje A, Danko CG, Mishmar D. 2017. Initiation of mtDNA transcription is followed by pausing, and diverges across human cell types and during evolution. Genome Res. 27:362-373.
- Bratic I, Hench J, Henriksson J, Antebi A, Bürglin TR, et al. 2009. Mitochondrial DNA level, but not active replicase, is essential for Caenorhabditis elegans development. Nucleic Acids Res. 37:1817–1828.
- Bratic I, Hench J, Trifunovic A. 2010. Caenorhabditis elegans as a model system for mtDNA replication defects. Methods. 51:437-443.
- Brown WM, George M, Wilson AC. 1979. Rapid evolution of animal mitochondrial DNA. Proc Natl Acad Sci USA. 76:1967-1971.
- Broz AK, Waneka G, Wu Z, Gyorfy MF, Sloan DB. 2021. Detecting de novo mitochondrial mutations in angiosperms with highly divergent evolutionary rates. Genetics. 218:iyab039.
- Cheng KC, Cahill DS, Kasai H, Nishimura S, Loeb LA. 1992. 8-Hydroxyguanine, an abundant form of oxidative DNA damage, causes $G \rightarrow T$ and $A \rightarrow C$ substitutions. J Biol Chem. 267:166–172.
- Cluett TJ, Akman G, Reyes A, Kazak L, Mitchell A, et al. 2018. Transcript availability dictates the balance between strand-asynchronous and strand-coupled mitochondrial DNA replication. Nucleic Acids Res. 46:10771-10781.
- D'Souza AR, Minczuk M. 2018. Mitochondrial transcription and translation: overview. Essays Biochem. 62:309-320.
- DeBalsi KL, Hoff KE, Copeland WC. 2017. Role of the mitochondrial DNA replication machinery in mitochondrial DNA mutagenesis, aging and age-related diseases. Ageing Res Rev. 33:89-104.

- Denver DR, Morris K, Lynch M, Vassilieva LL, Thomas WK. 2000. High direct estimate of the mutation rate in the mitochondrial genome of Caenorhabditis elegans. Science. 289:2342-2344.
- Denver DR, Morris K, Lynch M, Thomas WK. 2004. High mutation rate and predominance of insertions in the Caenohabditis elegans nuclear genome. Nature. 430:679-682.
- Denver DR, Wilhelm LJ, Howe DK, Gafner K, Dolan PC, et al. 2012. Variation in base-substitution mutation in experimental and natural lineages of caenorhabditis nematodes. Genome Biol Evol. 4: 513-522.
- Falkenberg M. 2018. Mitochondrial DNA replication in mammalian cells: overview of the pathway. Essays Biochem. 62:287-296.
- Fan W, Waymire KG, Narula N, Li P, Rocher C, et al. 2008. A mouse model of mitochondrial disease reveals germline selection against severe mtDNA mutations. Science. 319:958-962.
- Frith MC. 2011. Gentle masking of low-complexity sequences improves homology search. PLoS One. 6:e28819.
- Gaillard H, Aguilera A. 2016. Transcription as a threat to genome integrity. Annu Rev Biochem. 85:291-317.
- Gemmell NJ, Metcalf VJ, Allendorf FW. 2004. Mother's curse: the effect of mtDNA on individual fitness and population viability. Trends Ecol Evol. 19:238-244.
- Gorelick AN, Kim M, Chatila WK, La K, Hakimi AA, et al. 2021. Respiratory complex and tissue lineage drive recurrent mutations in tumour mtDNA. Nat Metab. 3:558-570.
- Gruber J, Ng LF, Fong S, Wong YT, Koh SA, et al. 2011. Mitochondrial changes in ageing Caenorhabditis elegans - what do we learn from superoxide dismutase knockouts? PLoS One. 6:e19444.
- Haag-Liautard C, Coffey N, Houle D, Lynch M, Charlesworth B, et al. 2008. Direct estimation of the mitochondrial DNA mutation rate in Drosophila melanogaster. PLoS Biol. 6:e204.
- Halsne R, Esbensen Y, Wang W, Scheffler K, Suganthan R, et al. 2012. Lack of the DNA glycosylases MYH and OGG1 in the cancer prone double mutant mouse does not increase mitochondrial DNA mutagenesis. DNA Repair (Amst). 11:278-285.
- Harman D. 1972. The biologic clock: the mitochondria? J Am Geriatr Soc. 20:145-147.
- Havird JC, Sloan DB. 2016. The roles of mutation, selection, and expression in determining relative rates of evolution in mitochondrial versus nuclear genomes. Mol Biol Evol. 33:3042-3053.
- Hazkani-Covo E, Zeller RM, Martin W. 2010. Molecular poltergeists: Mitochondrial DNA copies (numts) in sequenced nuclear genomes. PLoS Genet. 6:e1000834.
- He F. 2011. Common worm media and buffers. Bio-Protocol. 1:7.
- Held JP, Patel MR. 2020. Functional conservation of mitochondrial RNA levels despite divergent mtDNA organization. BMC Res Notes. 13:334.
- Hood WR, Williams AS, Hill GE. 2019. An ecologist's guide to mitochondrial DNA mutations and senescence. Integr Comp Biol. 59:
- Howe DK, Baer CF, Denver DR. 2010. High rate of large deletions in Caenorhabditis briggsae mitochondrial genome mutation processes. Genome Biol Evol. 2:29-38.
- Itsara LS, Kennedy SR, Fox EJ, Yu S, Hewitt JJ, et al. 2014. Oxidative stress is not a major contributor to somatic mitochondrial DNA mutations. PLoS Genet. 10:e1003974.
- Jõers P, Jacobs HT. 2013. Analysis of replication intermediates indicates that Drosophila melanogaster mitochondrial DNA replicates by a strand-coupled theta mechanism. PLoS One. 8:e53249.
- Ju YS, Alexandrov LB, Gerstung M, Martincorena I, Nik-Zainal S, et al. 2014. Origins and functional consequences of somatic mitochondrial DNA mutations in human cancer. eLife. 3:e02935.

- Katju V, Bergthorsson U. 2019. Old trade, new tricks: Insights into the spontaneous mutation process from the partnering of classical mutation accumulation experiments with high-throughput genomic approaches. Genome Biol Evol. 11:136-165.
- Kauppila JHK, Bonekamp NA, Mourier A, Isokallio MA, Just A, et al. 2018. Base-excision repair deficiency alone or combined with increased oxidative stress does not increase mtDNA point mutations in mice. Nucleic Acids Res. 46:6642-6649.
- Keightley PD, Trivedi U, Thomson M, Oliver F, Kumar S, et al. 2009. Analysis of the genome sequences of three Drosophila melanogaster spontaneous mutation accumulation lines. Genome Res. 19:1195-1201.
- Kennedy SR, Salk JJ, Schmitt MW, Loeb LA. 2013. Ultra-sensitive sequencing reveals an age-related increase in somatic mitochondrial mutations that are inconsistent with oxidative damage. PLoS Genet. 9:e1003794.
- Kennedy SR, Schmitt MW, Fox EJ, Kohrn BF, Salk JJ, et al. 2014. Detecting ultralow-frequency mutations by Duplex Sequencing. Nat Protoc. 9:2586-2606.
- Kino K, Hirao-Suzuki M, Morikawa M, Sakaga A, Miyazawa H. 2017. Generation, repair and replication of guanine oxidation products. Genes Environ. 39:21.
- Kirkwood TBL, Kowald A. 2012. The free-radical theory of ageing older, wiser and still alive: Modelling positional effects of the primary targets of ROS reveals new support. Bioessays. 34:692-700.
- Kono N, Tomita M, Arakawa K. 2018. Accelerated laboratory evolution reveals the influence of replication on the GC skew in Escherichia coli. Genome Biol Evol. 10:3110-3117.
- Konrad A, Thompson O, Waterston RH, Moerman DG, Keightley PD, et al. 2017. Mitochondrial mutation rate, spectrum and heteroplasmy in Caenorhabditis elegans spontaneous mutation accumulation lines of differing population size. Mol Biol Evol. 34:
- Krašovec R, Richards H, Gifford DR, Hatcher C, Faulkner KJ, et al. 2017. Spontaneous mutation rate is a plastic trait associated with population density across domains of life. PLoS Biol. 15:e2002731.
- Kreutzer DA, Essigmann JM. 1998. Oxidized, deaminated cytosines are a source of $C \rightarrow T$ transitions in vivo. Proc Natl Acad Sci USA. 95:3578-3582.
- Krzywinski M, Schein J, Birol I, Connors J, Gascoyne R, et al. 2009. Circos: an information aesthetic for comparative genomics. Genome Res. 19:1639-1645.
- Langmead B, Salzberg SL. 2012. Fast gapped-read alignment with Bowtie 2. Nat Methods. 9:357-359.
- Lemire B. 2005. Mitochondrial genetics, in WormBook: the online review of C. elegans biology, The C. elegans Research Community. pp. 1–10.
- Lewis SC, Joers P, Willcox S, Griffith JD, Jacobs HT, et al. 2015. A rolling circle replication mechanism produces multimeric lariats of mitochondrial DNA in Caenorhabditis elegans. PLoS Genet. 11:e1004985.
- Ling F, Niu R, Hatakeyama H, Goto YI, Shibata T, et al. 2016. Reactive oxygen species stimulate mitochondrial allele segregation toward homoplasmy in human cells. Mol Biol Cell. 27:1684-1693.
- Ling F, Yoshida M. 2020. Rolling-circle replication in mitochondrial dna inheritance: scientific evidence and significance from yeast to human cells. Genes (Basel). 11:514.
- Liu H, Zhang J. 2020. Higher germline mutagenesis of genes with stronger testis expressions refutes the transcriptional scanning hypothesis. Mol Biol Evol. 37:3225-3231.
- Longley MJ, Nguyen D, Kunkel TA, Copeland WC. 2001. The fidelity of human DNA polymerase γ with and without Exonucleolytic proofreading and the p55 accessory subunit. J Biol Chem. 276: 38555-38562.

- Longley MJ, Graziewicz MA, Bienstock RJ, Copeland WC. 2005. Consequences of mutations in human DNA polymerase γ . Gene. 354:125-131.
- Lynch M, Ackerman MS, Gout JF, Long H, Sung W, et al. 2016. Genetic drift, selection and the evolution of the mutation rate. Nat Rev Genet. 17:704-714.
- Marni JF, Soondhiemer N. 2010. Mitochondrial genetic diseases. Curr Opin Pediatr. 22:711-716.
- Martin M. 2011. Cutadapt removes adapter sequences from high-throuoghput sequencing reads. EMBnet J. 17:10-12.
- Melvin RG, Ballard JWO. 2017. Cellular and population level processes influence the rate, accumulation and observed frequency of inherited and somatic mtDNA mutations. Mutagenesis. 32:
- Miquel J, Economos AC, Fleming J, Johnson JE. 1980. Mitochondrial role in cell aging. Exp Gerontol. 15:575-591.
- Molnar RI, Bartelmes G, Dinkelacker I, Witte H, Sommer RJ. 2011. Mutation rates and intraspecific divergence of the mitochondrial genome of pristionchus pacificus. Mol Biol Evol. 28:2317-2326.
- Monzio Compagnoni G, Di Fonzo A, Corti S, Comi GP, Bresolin N, et al. 2020. The role of mitochondria in neurodegenerative diseases: the lesson from Alzheimer's disease and Parkinson's disease. Mol Neurobiol. 57:2959-2980.
- Murphy MP. 2009. How mitochondria produce reactive oxygen species. Biochem J. 417:1-13.
- Nabel CS, Manning SA, Kohli RM. 2012. The curious chemical biology of cytosine: deamination, methylation, and oxidation as modulators of genomic potential. ACS Chem Biol. 7:20-30.
- Ng LF, Ng LT, Van Breugel M, Halliwell B, Gruber J. 2019. Mitochondrial DNA damage does not determine C. Elegans lifespan. Front Genet. 10:311.
- Ni T, Wei G, Shen T, Han M, Lian Y, et al. 2015. MitoRCA-seq reveals unbalanced cytocine to thymine transition in Polg mutant mice. Sci Rep. 5:12049.
- Okimoto R, Macfarlane JL, Clary DO, Wolstenholme DR. 1992. The mitochondrial genomes of two nematodes, Caenorhabditis elegans and Ascaris suum. Genetics. 130:471-498.
- Poetsch AR, Boulton SJ, Luscombe NM. 2018. Genomic landscape of oxidative DNA damage and repair reveals regioselective protection from mutagenesis 06 Biological Sciences 0604 Genetics. Genome Biol. 19:215.
- Raamsdonk JMV, Hekimi S. 2009. Deletion of the mitochondrial superoxide dismutase sod-2 extends lifespan in Caenorhabditis elegans. PLoS Genet. 5:e1000361.https://doi.org/10.1371/journal. pgen.1000361
- Rajaei M, Saxena AS, Johnson LM, Snyder MC, Crombie TA, et al. 2021. Mutability of mononucleotide repeats, not oxidative stress, explains the discrepancy between laboratory-accumulated mutations and the natural allele-frequency spectrum in C. elegans. bioRxiv. https://doi.org/10.1101/2021.02.09.430480
- Richly E, Leister D. 2004. NUMTs in sequenced eukaryotic genomes. Mol Biol Evol. 21:1081-1084.
- Richter C, Park JW, Ames BN. 1988. Normal oxidative damage to mitochondrial and nuclear DNA is extensive. Proc Natl Acad Sci USA. 85:6465-6467.
- Salk JJ, Schmitt MW, Loeb LA. 2018. Enhancing the accuracy of next-generation sequencing for detecting rare and subclonal mutations. Nat Rev Genet. 19:269-285.
- Samstag CL, Hoekstra JG, Huang CH, Chaisson MJ, Youle RJ, et al. 2018. Deleterious mitochondrial DNA point mutations are overrepresented in Drosophila expressing a proofreading-defective DNA polymerase γ. PLoS Genet. 14:e1007805.

- Sanchez-Contreras M, Sweetwyne MT, Hipp MJ, Kohrn BF, Schmidt EK, et al. 2021. A mutational gradient drives somatic mutation accumulation in mitochondrial DNA and influences germline polymorphisms and genome composition. bioRxiv. doi:10.1101/2021.06.18.448725
- Schaack S, Ho EKH, MacRae F. 2020. Disentangling the intertwined roles of mutation, selection and drift in the mitochondrial genome. Philos Trans R Soc Lond B Biol Sci. 375:20190173.
- Schirmer M, D'Amore R, Ijaz UZ, Hall N, Quince C. 2016. Illumina error profiles: resolving fine-scale variation in metagenomic sequencing data. BMC Bioinformatics. 17:125.
- Schmitt MW, Kennedy SR, Salk JJ, Fox EJ, Hiatt JB, et al. 2012. Detection of ultra-rare mutations by next-generation sequencing. Proc Natl Acad Sci USA. 109:14508–14513.
- Shigenaga MK, Hagen TM, Ames BN. 1994. Oxidative damage and mitochondrial decay in aging. Proc Natl Acad Sci USA. 91:10771–10778.
- Sloan DB, Broz AK, Sharbrough J, Wu Z. 2018. Detecting rare mutations and DNA damage with sequencing-based methods. Trends Biotechnol. 36:729–740.
- Szczepanowska K, Trifunovic A. 2015. Different faces of mitochondrial DNA mutators. Biochim Biophys Acta. 1847:1362–1372.
- Thompson O, Edgley M, Strasbourger P, Flibotte S, Ewing B, et al. 2013. The million mutation project: a new approach to genetics in *Caenorhabditis elegans*. Genome Res. 23:1749–1762.
- Uchimura A, Higuchi M, Minakuchi Y, Ohno M, Toyoda A, et al. 2015. Germline mutation rates and the long-term phenotypic effects of mutation accumulation in wild-type laboratory mice and mutator mice. Genome Res. 25:1125–1134.
- Wagner JT, Howe DK, Estes S, Denver DR. 2020. Mitochondrial DNA variation and selfish propagation following experimental bottlenecking in two distantly related *Caenorhabditis briggsae* isolates. Genes (Basel). 11:77.
- Wai T, Ao A, Zhang X, Cyr D, Dufort D, et al. 2010. The role of mitochondrial DNA copy number in mammalian fertility. Biol Reprod. 83:52–62.

- Waneka G, Vasquez YM, Bennett GM, Sloan DB. 2021. Mutational pressure drives differential genome conservation in two bacterial endosymbionts of sap-feeding insects. Genome Biol Evol. 13: evaa254.
- Wang C, McPherson JR, Zhang LH, Rozen S, Sabapathy K. 2016. Transcription-associated mutation of lasR in *Pseudomonas aeruginosa*. DNA Repair (Amst). 46:9–19.
- Weller AM, Rödelsperger C, Eberhardt G, Molnar RI, Sommer RJ. 2014. Opposing forces of A/T-biased mutations and G/C-biased gene conversions shape the genome of the nematode *Pristionchus pacificus*. Genetics. 196:1145–1152.
- Wolfe KH, Li WH, Sharp PM. 1987. Rates of nucleotide substitution vary greatly among plant mitochondrial, chloroplast, and nuclear DNAs. Proc Natl Acad Sci USA. 84:9054–9058.
- Wu Z, Waneka G, Broz AK, King CR, Sloan DB. 2020. MSH1 is required for maintenance of the low mutation rates in plant mitochondrial and plastid genomes. Proc Natl Acad Sci USA. 117:16448–16455.
- Xu S, Schaack S, Seyfert A, Choi E, Lynch M, et al. 2012. High mutation rates in the mitochondrial genomes of *Daphnia pulex*. Mol Biol Evol. 29:763–769. doi:10.1093/molbev/msr243
- Yang S, Feng X, Jiao Z, Lu D, Duan M, et al. 2016. The complete mitochondrial genome of Caenorhabditis remanei (Rhabditida: Rhabditoidae), in comparison with four other Caenorhabditis species. Gene Reports. 5:1–9.
- Yasukawa T, Reyes A, Cluett TJ, Yang MY, Bowmaker M, et al. 2006. Replication of vertebrate mitochondrial DNA entails transient ribonucleotide incorporation throughout the lagging strand. EMBO J. 25:5358–5371.
- Zheng W, Khrapko K, Coller HA, Thilly WG, Copeland WC. 2006. Origins of human mitochondrial point mutations as DNA polymerase γ -mediated errors. Mutat. Res. Fundam. Mutat Res. 599: 11–20.

Communicating editor: J. A. Surtees